npj | climate and atmospheric science

Article

Published in partnership with CECCR at King Abdulaziz University

https://doi.org/10.1038/s41612-026-01377-w

Anthropogenic aerosols can shape the winter mid-latitude cyclone tracks

Dianbin Cao[1], Dongze Xu[2], Yanluan Lin[2] ✉, Yi Deng[3] ✉, Xuelong Chen[4], Qiang Zhang[2], Meng Gao[5] & Xu Zhang[6]

Mid-latitude cyclones are "parent storms" of various weather hazards and contribute significantly to the moisture and heat intrusion into the Arctic. Anthropogenic aerosols are known to affect cyclone intensities and their associated precipitation, but their impacts on cyclone tracks remain largely unclear. Here, based on both observational data diagnosis and global climate model simulations, we show that anthropogenic aerosols over East Asia can lead to a significant poleward drift of mid-latitude cyclone tracks in winter over the North Pacific. By suppressing precipitation in the southeastern sector of cyclones and enhancing it in the northeastern sector, aerosols increase the positive potential vorticity tendency northeast of the cyclones, thereby driving their poleward drift. This might give rise to more cyclones migrating into the Arctic over the North Pacific, reducing the Arctic sea ice extent in recent decades. In the future, efforts to reduce aerosol emissions in East Asia could potentially mitigate the poleward migration of the storm track driven by global warming.

Mid-latitude cyclones generate most of the day-to-day weather variability and play an important role in meridional heat and moisture transport[1–3]. They exert large socioeconomic impacts through attendant weather hazards. Atmospheric aerosols, via their direct radiative effect and indirect cloud-precipitation associated effect, can influence mid-latitude cyclones via sophisticated multi-scale processes through modulation of convection and large-scale waves[4–6]. Spatially- and temporally-varying aerosol distribution and properties also add to the complexity of interaction with mid-latitude cyclones[7–9].

Several studies have suggested that aerosols may change meridional temperature gradient, jet location and mid-latitude cyclone activity via the aerosol-radiation interactions[10–12]. Aerosols can also change cloud and precipitation distribution through participating in cloud and precipitation microphysical processes, suppressing and delaying warm-phase precipitation[13–15] and invigorating convections associated with the cold/warm front of mid-latitude cyclones[16–19]. Higher aerosol concentrations tend to increase the intensity and precipitation of mid-latitude cyclones[5,17,18,20]. Although impacts of aerosols on the number, intensity and precipitation of mid-latitude cyclones have been explored, their impacts on the track and movement of mid-latitude cyclones remain elusive.

It has been deemed that small deviations in the location of cyclone tracks can result in tremendous impacts on the midlatitude and Arctic climate[21–23]. In this context, we explore a potential linkage between anthropogenic aerosols and cyclone movement based on a Lagrangian cyclone tracking method (see "Methods"). We focus on the impacts of anthropogenic aerosol emissions over East Asia on North Pacific boreal winter cyclone tracks as well as the potential interactions with storm development downstream.

Results

Enhanced poleward migration of mid-latitude cyclones over the North Pacific

Aerosol outflows from the East Asian continent have been noted to increase significantly during the period 2000-2014 (Figs. S1a and S2) based on atmospheric field measurements and satellite observations[17,24,25]. Aerosol optical depth (AOD) has increased significantly over East Asia (EA, 22°N ~ 44°N, 110°E ~ 124°E, red box in Fig. S1) after 2000 based on MERRA-2 (Modern-Era Retrospective analysis for Research and Applications, Version 2) reanalysis[26], which has a good correspondence with MODIS AOD after 2000 (Fig. S2). Here, we focus on the cyclones generated in a region more susceptible to high aerosol concentrations (green box in

[1]Alpine Paleoecology and Human Adaptation Group (ALPHA), State Key Laboratory of Tibetan Plateau Earth System, Environment and Resources (TPESER), Institute of Tibetan Plateau Research, Chinese Academy of Sciences, Beijing, China. [2]Ministry of Education Key Laboratory for Earth System Modeling, Department of Earth System Science, Tsinghua University, Beijing, China. [3]School of Earth and Atmospheric Sciences, Georgia Institute of Technology, Atlanta, GA, USA. [4]Land-Atmoshere Interaction and its Climatic Effects Group, State Key Laboratory of Tibetan Plateau Earth System, Environment and Resources (TPESER), Institute of Tibetan Plateau Research, Chinese Academy of Sciences, Beijing, China. [5]Department of Geography, Hong Kong Baptist University, Hong Kong SAR, China. [6]Ice Dynamics and Paleoclimate, British Antarctic Survey, Cambridge, UK. ✉e-mail: yanluan@tsinghua.edu.cn; yi.deng@eas.gatech.edu

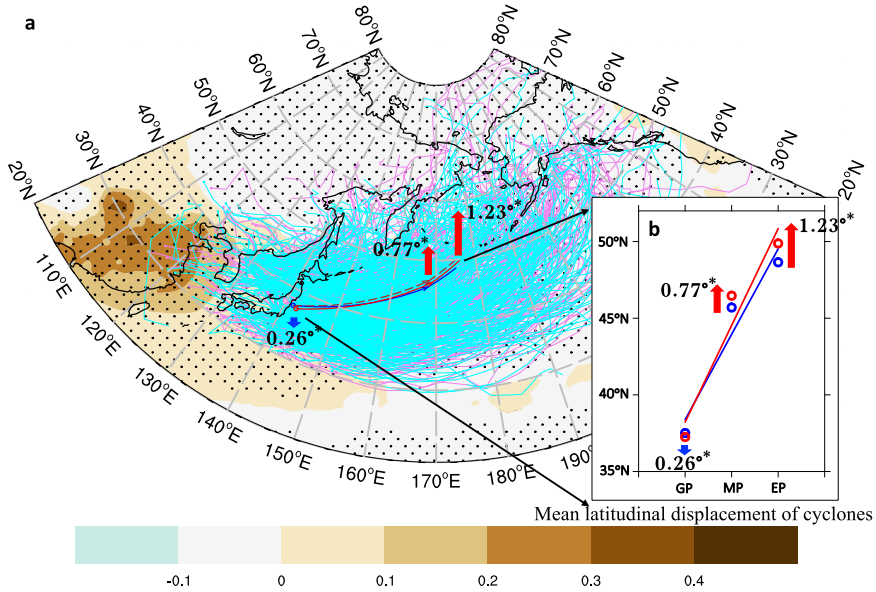

Fig. 1 | Polar shift of mid-latitude cyclone tracks in East Asia. a The tracks of mid-latitude cyclones generated in the area (30°N ~ 45°N, 110°E ~ 160°E) in DJF in High-AOD years (purple lines) and Low-AOD years (light blue lines) over the period 1980-2020. The thick red and blue lines are their average. The brown dashed line indicates a translation of the average High-AOD track to the starting point of the average Low-AOD track, highlighting their spatial displacement. The arrows and fonts indicate the movement directions and magnitudes of the generation, maximum intensity and end points of cyclones between High-AOD years and Low-AOD years, respectively. The asterisk indicates statistical significance at the $p < 0.1$ level. The shading indicates the AOD difference between the two periods. **b** An enlarged view of the average shift latitudes of the generation, maximum intensity and end points of cyclones in (**a**). Stippling indicates areas where the differences are statistically significant at the $p < 0.1$ level based on a Student's t test.

Fig. S1, 30°N ~ 45°N, 110°E ~ 160°E). The average track of mid-latitude cyclones during Northern Hemisphere wintertime (December–February, DJF) in 15 High-AOD years (red line in Fig. 1) shows a distinct northeastward shift (hereafter referred to as the poleward shift) relative to that in 15 Low-AOD years (blue line in Fig. 1) over the past four decades. Specifically, it is only 0.26° apart (37.25°N vs. 37.51°N) for the average cyclone genesis location, but it increased to 0.77° and 1.23° further north for the cyclone maximum intensity (measured by minimum SLP) and end point, respectively, in the High-AOD years compared to the Low-AOD years. Quantitatively, there are 49 cyclones (7.09% of the total) crossing 65°N in the High-AOD years. In contrast, there are only 27 cyclones (3.91% of the total) crossing 65°N in the Low-AOD years. For cyclones generated in a larger region (blue box, 30°N ~ 50°N, 110°E ~ 180°E, Fig. S1a) with a smaller average AOD, the magnitude of the poleward shift decreased (Fig. S3a), which provided further evidence for possible aerosol impacts on the cyclone track shift. Here, it should be cautioned that such a distinct northward shift of cyclone tracks might not be solely related to increased aerosols, since other factors, such as atmospheric teleconnections, background baroclinicity and sea surface temperature (SST), might also play a role[27–31].

Aerosol-induced poleward migration of cyclones in model simulations

A pair of 54-year AMIP-type simulations were conducted using Community Atmosphere Model version 5.3 (CAM5) with different anthropogenic aerosol emissions to investigate aerosol impacts on the cyclone tracks over the North Pacific in winter. One used prescribed CMIP5 aerosol emissions (EXP_CTRL), and the other used tenfold emissions (EXP_10F) over East Asia with the same boundary conditions, including prescribed climatological SST and sea ice concentrations. Note that simulated AOD over East Asia and surrounding regions in EXP_10F is much closer to that of MODIS, especially in the key region for this study (Fig. S1a, c). This suggests that CAM5 effectively captures the spatial distribution of East Asian aerosols[32], despite the certain degree of overestimation in the aerosol magnitude (Fig. S1). To identify the possible impact of global warming on cyclone tracks, an additional 54-year simulationwas conducted. The simulation is the same as EXP_CTRL, except for using the global mean sea surface temperature from the 15 High-AOD years (EXP_CTRL_HSST). These simulations used the climatological boundary conditions without interannual variability, allowing each year to be treated as an independent sample to isolate the influence of internal climate variability. More details of the simulation configurations can be found in the methods.

Compared to EXP_CTRL, the cyclone track density in EXP_10F shows a significant decrease over the east-central North Pacific, while it increases over the northwestern region near Japan and extends into the Bering Sea (Fig. 2a, b). Such a track shift also manifests clearly in the distribution of precipitation (Fig. 2c). Precipitation increases significantly in the northwest North Pacific (up to 0.4 mm/day near Japan) and decreases in the southeast North Pacific (~0.8 mm/day). Note that cyclone precipitation is dominated by large-scale precipitation rather than convection precipitation (Fig. S4), which is modulated by aerosols in CAM5. In addition, the mid-latitude jet at 200 hPa also presents a poleward shift, with a positive anomaly in high latitudes and a negative anomaly in mid-latitudes over the North Pacific in EXP_10F (Fig. 2d). Specifically, a distinct poleward shift of cyclone activities over the North Pacific was noted in EXP_10F (Fig. 2b) for cyclones generated within the region of interest (30°N ~ 45°N, 110°E ~ 160°E). The average location of storm maximum intensity and end point significantly ($p < 0.1$) shifts northward by 0.74° and 0.92° (0.5° and 0.68° for cyclones in the blue box with lower average aerosol burden in Fig. S1d; see Fig. S3b) degrees of latitude in EXP_10F compared to EXP_CTRL. In addition, consistent with observations, the average location of cyclogenesis (the start point of the track) between EXP_CTRL and EXP_10F is similar, probably because aerosols have not been strongly involved in cyclone development at this stage. In the EXP_CTRL_HSST (a warmer climate context, see method sector), the cyclone track has a minor poleward shift, an average of about 0.09°, in Fig. S3c. The result generally aligns with previous studies, which found that the cyclone track shifts northward by approximately 0.12° for a 0.5 K increase in global mean surface temperature[33]. The above results indicate a more dominant impact of aerosols on mid-latitude cyclone tracks under global warming (Fig. S3). These simulations confirm the robustness of the northward shift of cyclones by increased aerosols noted in observations.

Mechanisms underlying aerosol-induced poleward migration of cyclones

The movement of cyclones is regulated by the large-scale steering flow and internal dynamic and thermodynamic structure of cyclones[34–36]. Two dominant mechanisms for the poleward movement of mid-latitude cyclones have been identified: horizontal advection of potential vorticity (PV) and PV generation associated with latent heat release (LHR)[33,37]. A classic picture is that a positive (negative) PV tendency located on the northeastern (southwestern) side of the cyclone, arising from both PV advection and latent heating-induced PV generation, contributes to an

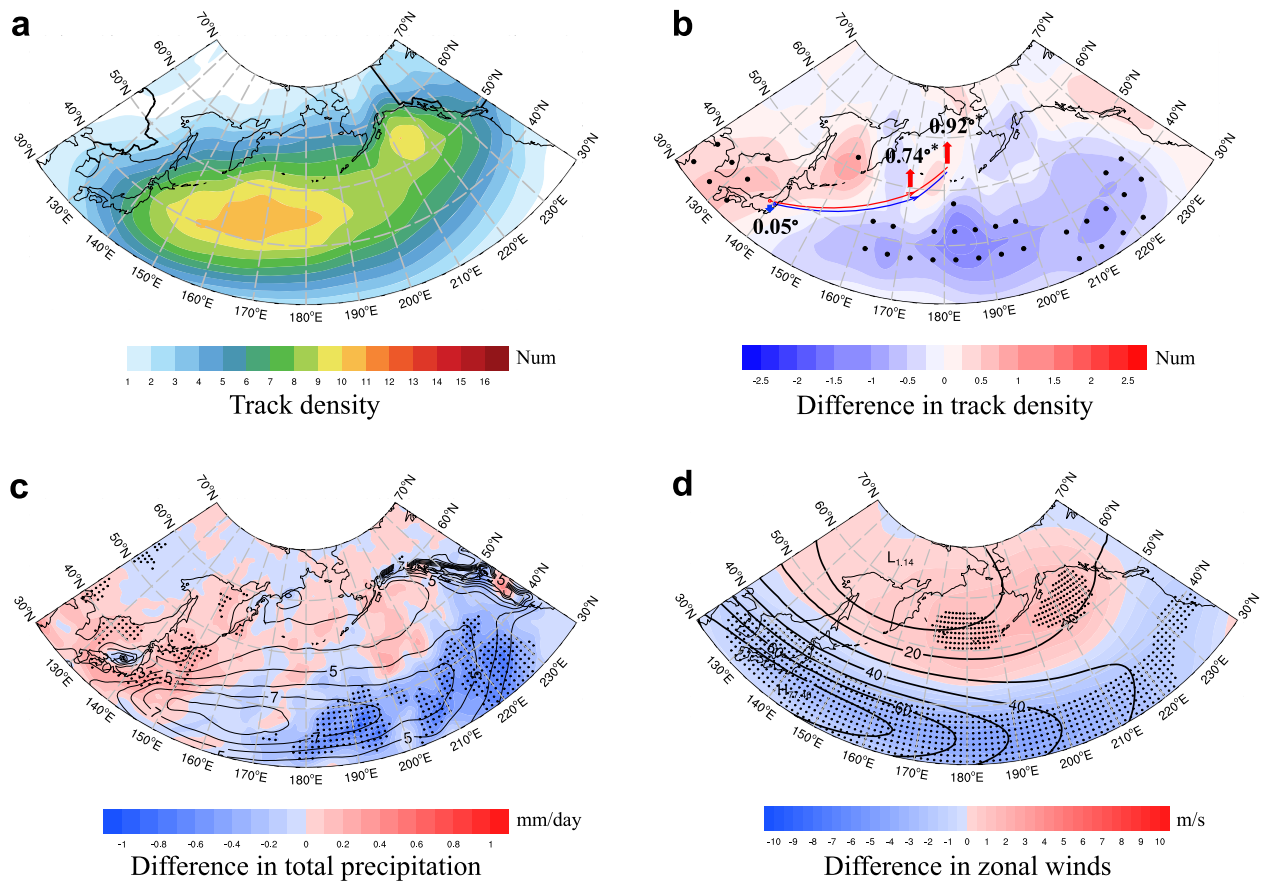

Fig. 2 | Polar shift of mid-latitude cyclone tracks caused by East Asian aerosols. **a** The DJF-mean track density of mid-latitude cyclones (unit: number in a 5°×5° grid) in EXP_CTRL. **b** The difference in the DJF-mean cyclone track density between EXP_10F and EXP_CTRL. The lines, arrows and fonts are the same as those in Fig. 1a except for simulation results. The asterisk indicates statistical significance at the $p < 0.1$ level. **c** The difference in DJF-mean total precipitation (unit: mm day^{-1}) between EXP_10F and EXP_CTRL. The black contours indicate the DJF-mean climatological total precipitation in EXP_CTRL. **d** Same as **c** except for the zonal wind (unit: m s^{-1}) at 200 hPa. "H" and "L" indicate the high and low centers of the climatological zonal wind, respectively. Stippling indicates areas where the differences are statistically significant at the $p < 0.1$ level based on a Student's t test.

overall eastward and poleward movement of cyclones[37]. In the following, a PV budget analysis was conducted on the cyclone composites (see "Methods").

Compared with EXP_CTRL, the dipole structure in the first and second quadrants of the PV advection field is clearly stronger in EXP_10F (Fig. 3a, d), which indicates an enhancement of meridional nonlinear advection (Fig. 3g). Thus, the nonlinear term produces a poleward tendency, leading to the poleward motion of the low-level cyclone[37]. Meanwhile, the magnitude of positive PV generation associated with latent heat release (LHR) also increases (Fig. 3b, e), with a clear dipole structure of PV changes associated with the enhanced warm front in northeast sector (Fig.3h). Collectively, these two factors—enhanced PV advection and intensified LHR-induced PV generation northeast of the cyclone—lead to an approximately 10% increase in the total PV tendency. Therefore, the total contribution is the stronger positive PV tendency in the northeast side of the cyclone, favoring a more poleward movement of cyclones in EXP_10F compared to EXP_CTRL (Fig. 3c, f, i).

Cyclone precipitation is concentrated in the northeast sector of the storm, featuring a typical "comma clouds" pattern characterized by warm frontal precipitation (Fig. 4a). The scenario of enhanced aerosol emission in EXP_10F produced more precipitation in the northeastern side of the cyclone and less precipitation in other regions than EXP_CTRL (Fig. 4b). Such an overall northeast shift of precipitation pattern well reflects the impacts of aerosol effects during the growth stage of the cyclone. A warm conveyor belt transports moist air originating from the cyclone's warm sector toward the warm front. High aerosol burden in the environment leads to the formation of more but smaller cloud droplets, suppressing rainfall formation along the conveyor belt through reduced auto-conversion and inhibited coalescence of cloud droplets into raindrops[38–40] (Fig. S5). This process reduces precipitation and moisture consumption south of the warm front and allows more moisture and cloud droplets to reach higher altitudes and higher latitudes, resulting in a larger total cloud fraction of the cyclone (Fig. 4c) and more latent heat release in the northeast quadrant of the cyclone in EXP_10F[41–43] (Fig. 4d). The extra heat release due to more water vapor condensation and/or cloud droplet freezing in the middle and upper troposphere led to the vertical temperature gradient change, increased instability, invigorated the vertical motion further downstream (Fig. 4c; see the anomalies in vertical motion anomaly in the 850–700 hPa layer and the total cloud fraction anomaly around 300hPa). The mechanism described above is similar to that noted in deep convection[44,45], but in a slantwise ascending fashion. As a result, precipitation along the warm conveyor belt increased downstream but decreased upstream, consistent with vertical motion changes (Fig. 4c). Consistently, LHR downstream is enhanced significantly with a broad peak from 850 to 600 hPa in EXP_10F compared to EXP_CTRL (Fig. 4d). Such a heating profile difference contributes to increased PV at lower levels with a decrease above 450 hPa (Fig. 4d). The position of the low-level positive PV anomaly favors northeast movement of the cyclone[33,37]. In addition, the negative PV anomaly strengthens the ridge

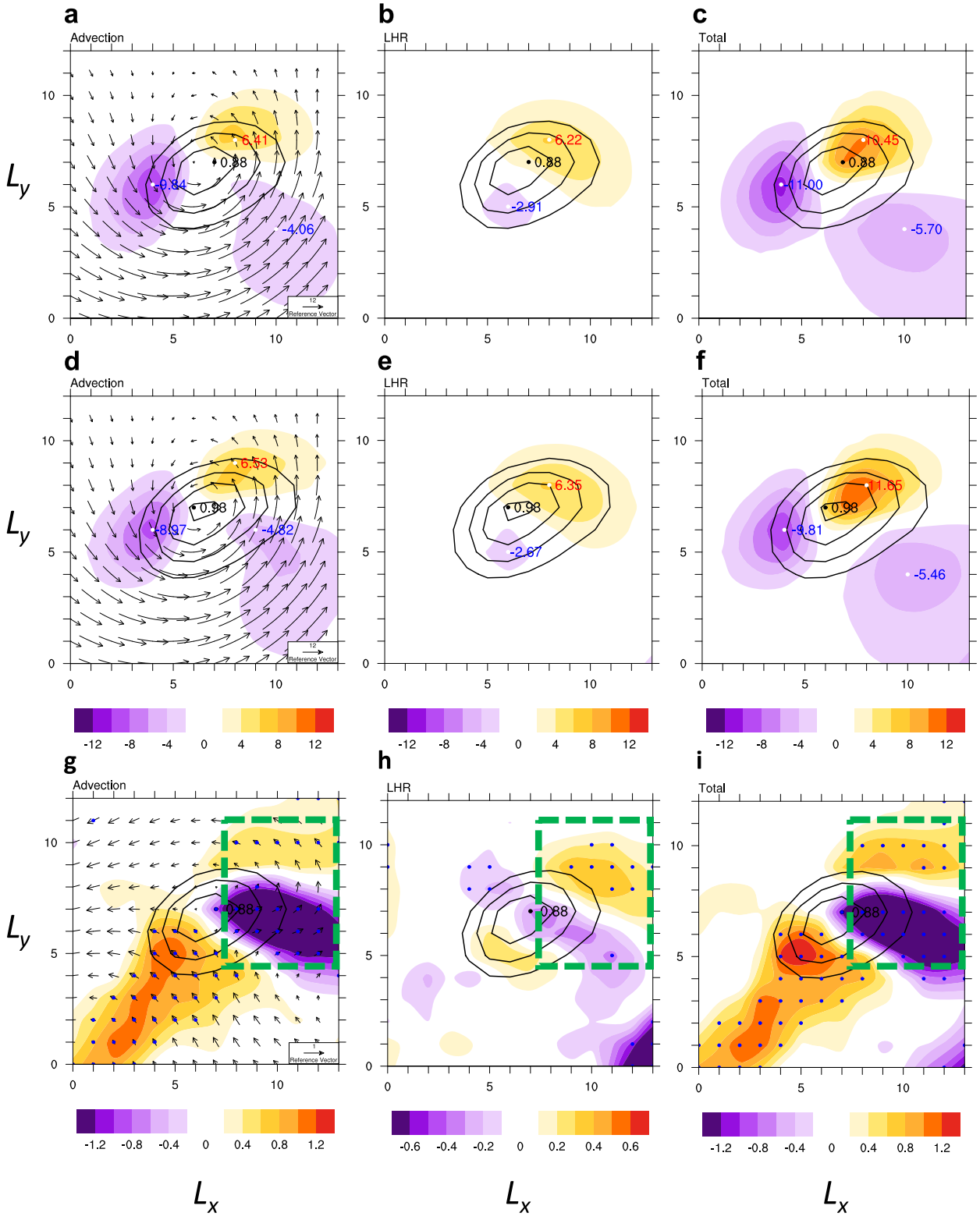

Fig. 3 | Composites of the cyclonic PV tendency. Horizontal PV advection (shaded) by low-level winds (black arrows) (**a**), PV tendency due to LHR (**b**), and total PV tendency (**c**) for EXP_CTRL at the level of 820 hPa. (**d-f**) Same as (**a–c**), but for EXP_10F. Black contours indicate the PV anomaly (unit: PVU), 1 PVU = 10^{-6} (K*m^2)/(kg*s). PV tendencies are expressed in units of 10^{-6} PVU s^{-1}. **g–i** Same as (**a–c**), except for the difference of EXP_10F minus EXP_CTRL. Blue stippling indicates areas where the differences are statistically significant at the $p < 0.1$ level based on a Student's t test.

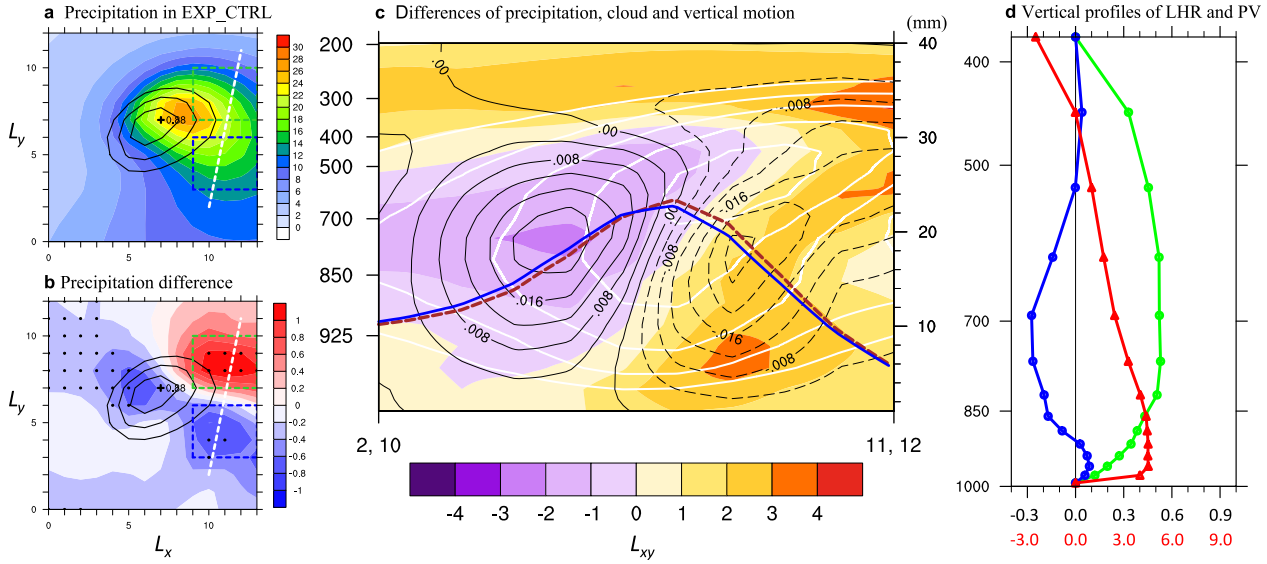

Fig. 4 | Changes in the cyclonic precipitation and vertical structure caused by aerosols. a The composite of cyclone precipitation in EXP_CTRL (unit: mm day^{-1}). **b** Same as (**a**), but for the difference in cyclone precipitation between EXP_10F and EXP_CTRL. The black contours in **a** and **b** indicate the PV anomaly at 820 hPa in EXP_CTRL. The black dots indicate the regions where the difference between EXP_CTRL and EXP_10F indicates statistical significance at the $p < 0.1$ level based on a Student's t test. **c** Cross sections of total cloud fraction in EXP_CTRL (white contours, unit: %), its differences (shaded), and vertical velocity (black contours, unit: Pa s^{-1}) between EXP_10F and EXP_CTRL along the white dashed line in (**a**, **b**). The blue (brown) line indicates the surface precipitation along the cross section (right y-axis) in EXP_CTRL (EXP_10F). **d** Vertical profiles of the latent heating rate (K day^{-1}, blue and green lines for regions within the blue and green boxes in (**b**), respectively) and PV anomaly (red line with a unit of 1 PVU for the green box in (**b**)) between EXP_10F and EXP_CTRL.

at upper levels with a deepening trough upstream caused by the large-scale dynamic adjustment processes. Subsequently, the strengthened upper-level PV dipole also favors the poleward motion of the low-level cyclone caused by the nonlinear advection of the low-level anomaly by the upper-level PV (Figs. 3d and S6) due to the westward tilted structure of mid-latitude cyclones with height[37]. LHR anomaly in the northeast of the cyclone enhanced the zonal temperature gradient, which led to the accelerated meridional advection east of cyclone, further transports warm and moist air to the north with more LHR northeast of the cyclone, providing a positive feedback promoting the poleward movement of the cyclone. Finally, both the LHR and the poleward advection by the upper-level PV are expected to be larger, which can lead to larger poleward deflection of storms (Fig. 5).

Discussion

Our findings indicate that aerosol emissions in East Asia can cause a significant poleward shift of the cyclone track over the western North Pacific by altering the PV tendency within the cyclone. In this sense, East Asia aerosols may have impacted the Arctic climate by affecting the mid-latitude cyclone tracks since these storms bring large amounts of moisture and energy into the Arctic. Actually, we noted a significant negative correlation ($p < 0.1$) between the numbers of mid-latitude cyclones entering the Arctic from the North Pacific and the sea ice extent of the Bering Sea from February to April, as well as a weak positive correlation at a statistically insignificant level ($p < 0.2$) between the cyclone numbers and AOD in East Asia (Fig. S7). Note that we mainly focused on the aerosol-cloud-precipitation effect in this study and have not attempted to isolate aerosol-radiation effect. Nevertheless, aerosol-radiation interaction could modulate the meridional temperature gradient (baroclinicity) and stability[9,12], and thus influence cyclone and storm track characteristics indirectly. Finally, it is important to emphasize that the impacts of aerosol on precipitation, clouds, and circulations are extremely complex. Therefore, more detailed observational analyses and modeling studies are necessary to better understand the effects of aerosols on mid-latitude cyclones and extratropical climate change in future work.

Methods

Data

The 6-hourly SLP fields of ERA-Interim reanalysis (~80 km) from 1979 to 2019[46], the monthly AOD of MODIS (0.1° × 0.1°) from 2000 to 2019[47], and MERRA-2 reanalysis (0.5° × 0.625°) from 1980 to 2019[26] are used for the evaluation of CAM5 simulations (0.9° × 1.25°) in terms of mid-latitude cyclone characteristics and aerosols. We used ERA-Interim reanalysis datasets instead of ERA5 (~31 km) in this study, primarily because its native horizontal resolution is more comparable to the simulated resolution of the CAM5 model (~100 km) to mitigate potential resolution-related effects. Here, we identified 15 years with larger AOD after 2000 (the High-AOD years) and 15 years with smaller AOD before 2000 (the Low-AOD years) over East Asia (22°N ~ 44°N, 110°E ~ 124°E) in winter (DJF) based on the MERRA-2 reanalysis and MODIS datasets (Fig. S2). Note that those years with large AOD before 2000 in MERRA-2 might be related to volcanic eruptions and thus were excluded.

Model simulations

The Community Atmosphere Model version 5.3 (CAM5) has been widely used for aerosol-related studies due to its comprehensive treatment of numerous complex aerosol processes, as well as aerosol physical, chemical, and optical properties[28,48,49]. Aerosol interactions with cloud and precipitation processes are well captured using the two-moment cloud microphysics[50,51] and a 3-mode modal aerosol module (MAM3)[32]. CAM5 can effectively simulate various aerosol direct and indirect effects on the radiation budget and the hydrological cycle[52]. More details of CAM5 can be found in Neale et al.[53].

In this study, CAM5 was integrated for 54 years using prescribed monthly mean climatological SST and sea ice during 1982–2000 with horizontal resolution of 0.9° × 1.25° and 30 vertically hybrid sigma-pressure levels. Three AMIP-type simulations with the climatological annual cycles

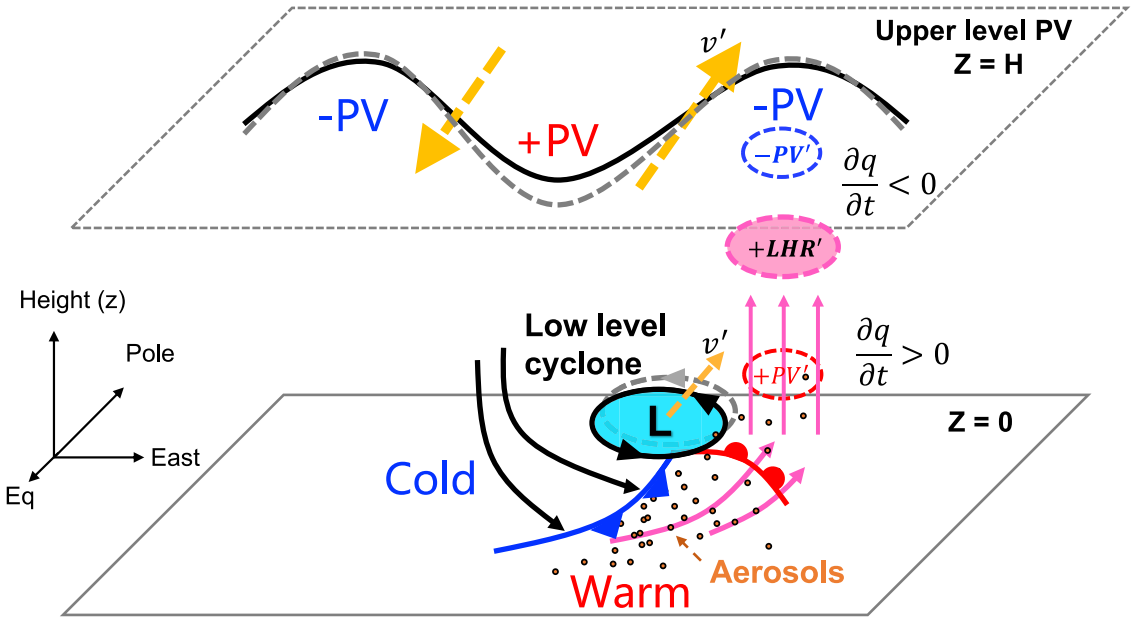

Fig. 5 | Schematic of the dynamical pathway of aerosol impacts on mid-latitude cyclone tracks. The two layers represent the upper layer (Z = H) and the surface (Z = 0). The black solid line at the upper layer denotes the upper-level PV wave. The gray dashed line shows the evolution of the black solid line. The light blue circle with "L" represents the low-level cyclone. The black and pink arrow lines indicate the cold, warm airflows and upward motion, respectively. The blue curved line with triangles and the red curved line with arches at the surface are the cold front and warm front. Brown dots represent aerosols. The dashed orange arrows and gray circle indicate the meridional wind anomaly and the low-level cyclone shift induced by aerosols, respectively. The dashed pink, blue and red ovals denote the LHR anomaly and the associated PV anomalies in the upper and lower troposphere, respectively.

of SST and sea ice concentrations were conducted. All simulations exclude the influence of internal climate variability. The control simulation (EXP_CTRL) used the default anthropogenic aerosol emissions from CMIP5[54]. Aerosol tenfold simulation (EXP_10F), identical to EXP_CTRL, but used tenfold anthropogenic aerosol emissions of EXP_CTRL over East Asia (22°N ~ 44°N, 100°E ~ 124°E, denoted by the red box in Fig. 1). Another simulation (EXP_CTRL_HSST) was identical to EXP_CTRL but used the average SST and sea ice from the 15 High-AOD years (2000–2014), representing a warmer climate context compared to 1982–2000, to examine the impacts of global warming on cyclone tracks.

CMIP5 severely underestimates anthropogenic aerosol emissions over East Asia in winter (DJF). Furthermore, the EXP_CTRL simulation underestimates aerosol optical depth (AOD) compared to the 17-year (2002–2018) averaged AOD observed by the Moderate Resolution Imaging Spectroradiometer (MODIS) Aqua satellite[47]. Such an underestimation has also been noted in previous studies, like Liu et al.[32]. Both EXP_CTRL and EXP_10F well capture the overall spatial distribution of AOD with MODIS, but with a better agreement with MODIS in terms of magnitude for EXP_10F (Fig. S1a, c ;see the green box). Note that the goal of this study is to quantify the aerosol impact on the downstream cyclone development and movement instead of the fidelity of the aerosol itself.

The first 3 years of CAM5 simulations are treated as the spin-up, and the cyclone tracking algorithm was applied to the remaining 51 years of simulations in winter (December to February, DJF). To evaluate the CAM5 simulation as well as the storm tracking algorithm, we apply the same tracking algorithm to 41 years (1979–2019) of ERA-Interim reanalysis[46]. Key storm characteristics—including intensity, duration, and track density—show reasonable agreement between CAM5 and ERA-Interim (Fig. S8), which is consistent with previous studies[10,55,56].

Cyclone tracking algorithm

We use sea level pressure (SLP) to identify the center of cyclones following Serreze[57] and Wang et al.[58]. Details of the storm-tracking algorithm are as follows: The cyclone center must have the SLP value smaller than its 24 enclosing grids within a region of 5 × 5 grids, and must satisfy the requirement that there is at least one closed isobar within an expanded 11 × 11 grid region. If multiple grids are found, the one with the largest Laplacian of SLP will be identified as the storm center. The track is then determined by connecting storm centers using a minimum distance method. The following criteria are applied to minimize occasional tracking errors: The storm's central pressure must fall below 1000 hPa at least once during its lifetime, its lifetime must exceed 24 h, the change in intensity must be less than 10 hPa over any 6-h period, the movement distance must be less than 700 km per 6 h, and the total traveling distance must exceed 1000 km.

PV tendency calculation

A potential vorticity (PV) budget is used to understand the mechanisms responsible for the poleward shift of mid-latitude cyclones caused by aerosols. From the perspective of PV analysis, two dominant mechanisms are responsible for the poleward movement tendency of mid-latitude cyclones: one is the advection terms of PV tendency involved in the beta-induced nonlinear meridional force[59,60], and the second is the diabatic heating terms associated with latent heat release (LHR)[33,37].

After neglecting the friction and internal dissipation, PV tendency related to the advection and LHR in pressure coordinates can be approximately given as

$$\frac{\partial q}{\partial t} = -\vec{u}\cdot\nabla q - \omega\frac{\partial q}{\partial p} - g\left(f\hat{k} + \nabla_p \times \vec{u}\right)\cdot\nabla_p\left(\frac{d\theta}{dt}\right)_{LHR}, \quad (1)$$

where q is PV, $\vec{u}$ is horizontal wind vector, ω is vertical velocity, p is atmospheric pressure, g is the gravitational acceleration, f is planetary vorticity, ∇_p is the gradient operator and θ is potential temperature. To calculate the contribution of LHR, here,

$$\left(\frac{d\theta}{dt}\right) = \omega\left(\frac{\partial\theta}{\partial p} - \frac{\gamma_m}{\gamma_d}\frac{\theta}{\theta_e}\frac{\partial\theta_e}{\partial p}\right), \quad (2)$$

Equation (2) was derived by Emanuel et al.[61] to estimate the contribution of latent heating. Here, θ_e is the equivalent potential temperature,

γ_m and γ_d represent the dry and moist lapse rates, respectively. Then, the PV tendency perturbation can be approximately written as

$$\frac{\partial q'}{\partial t} = -\bar{u}\frac{\partial q'}{\partial x} - v'\frac{\partial \bar{q}}{\partial y} - u'\frac{\partial q'}{\partial x} - v'\frac{\partial q'}{\partial y} - \omega\frac{\partial q}{\partial p} - g\left(f\hat{k} + \nabla_p \times \vec{u}\right) \cdot \nabla_p \left(\frac{d\theta}{dt}\right)_{LHR} \quad (3)$$

Where $\bar{u}$ is the background zonal flow, u' and v' is the zonal and meridional flow perturbation, respectively. $\bar{q}$ and q' is the background PV and PV perturbation.

Here, we produced the composites of the lower troposphere PV tendency (the level of 820 hPa was chosen as a representative for the analysis of PV tendency budget, and the results at other lower troposphere levels are similar) associated with the cyclones generated in the green box in Fig. S1. For each cyclone identified, the above PV analysis was conducted every 6 h within a box (14° latitude by 18° longitude) centering around the cyclone center during its growth stage in the green box in Fig. S1, namely, until its peak time. Over 12,500 samples were used to obtain the composites of PV tendency in Fig. 3. The composites were created by averaging the variables of each snapshot.

Data availability

The ERA-Interim, ERA5 and MERRA2 reanalysis datasets are available at https://www.ecmwf.int/en/forecasts/dataset/ecmwf-reanalysis-interim, https://cds.climate.copernicus.eu/datasets and https://disc.gsfc.nasa.gov/datasets, respectively. The MODIS data are acquired from https://disc.gsfc.nasa.gov/datasets.

Code availability

All figures are made by NCAR Command Language (Version 6.4.0), which is available at https://www.ncl.ucar.edu/. The scripts used in this study are available from the author upon request.

Received: 15 September 2025; Accepted: 3 March 2026;
Published online: 18 March 2026

References

1. Zapotocny, J. V. Relationships between available potential energy, kinetic energy, and extratropical cyclone activity within East Coast cyclogenetic regions. *J. Geophys. Res.* **92**, 8401–8410 (1987).
2. Fearon, M. G., Doyle, J. D., Ryglicki, D. R., Finocchio, P. M. & Sprenger, M. The role of cyclones in moisture transport into the arctic. *Geophys. Res. Lett.* **48**, e2020GL090353 (2021).
3. Dacre, H. F. & Clark, P. A. A kinematic analysis of extratropical cyclones, warm conveyor belts and atmospheric rivers. *Npj Clim. Atmos. Sci.* **8**, 97 (2025).
4. Ming, Y., Ramaswamy, V. & Chen, G. A model investigation of aerosol-induced changes in boreal winter extratropical circulation. *J. Clim.* **24**, 6077–6091 (2011).
5. Lu, Y. & Deng, Y. Initial transient response of an intensifying baroclinic wave to increases in cloud droplet number concentration. *J. Clim.* **28**, 9669–9677 (2015).
6. McCoy, D. T. et al. The aerosol-cyclone indirect effect in observations and high-resolution simulations. *Atmos. Chem. Phys.* **18**, 1–20 (2017).
7. Grandey, B. S., Stier, P., Wagner, T. M., Grainger, R. G. & Hodges, K. I. The effect of extratropical cyclones on satellite-retrieved aerosol properties over ocean. *Geophys. Res. Lett.* **38**, L13805 (2011).
8. Naud, C. M., Posselt, D. J. & van den Heever, S. C. Aerosol optical depth distribution in extratropical cyclones over the Northern Hemisphere oceans. *Geophys. Res. Lett.* **43**(10), 504–10,511 (2016).
9. Lin, Y., Zhang, J., Li, X. & Deng, Y. Response of eddy activities to localized diabatic heating in Held–Suarez simulations. *Clim. Dyn.* **51**, 3421–3434 (2018).
10. Geng, Q. & Sugi, M. Possible change of extratropical cyclone activity due to enhanced greenhouse gases and sulfate aerosols study with a high-resolution AGCM. *J. Clim.* **16**, 2262–2274 (2003).
11. Wang, Y. et al. Reduced European aerosol emissions suppress winter extremes over northern Eurasia. *Nat. Clim. Change* **10**, 225–230 (2020).
12. Kuntz, L. B. & Schrag, D. P. Impact of Asian aerosol forcing on tropical Pacific circulation and the relationship to global temperature trends. *J. Geophys. Res. Atmos.* **121**(14), 403–14,413 (2016).
13. Igel, A. L., van den Heever, S. C., Naud, C. M., Saleeby, S. M. & Posselt, D. J. Sensitivity of warm-frontal processes to cloud-nucleating aerosol concentrations. *J. Atmos. Sci.* **70**, 1768–1783 (2013).
14. Thompson, G. & Eidhammer, T. A study of aerosol impacts on clouds and precipitation development in a large winter cyclone. *J. Atmos. Sci.* **71**, 3636–3658 (2014).
15. Naud, C. M., Posselt, D. J. & van den Heever, S. C. Observed covariations of aerosol optical depth and cloud cover in extratropical cyclones: aerosol versus cloud in ETCs. *J. Geophys. Res. Atmos.* **122**, 338–10,356 (2017).
16. Zhang, R., Li, G., Fan, J., Wu, D. L. & Molina, M. J. Intensification of Pacific storm track linked to Asian pollution. *Proc. Natl. Acad. Sci. USA* **104**, 5295–5299 (2007).
17. Wang, Y., Zhang, R. & Saravanan, R. Asian pollution climatically modulates mid-latitude cyclones following hierarchical modelling and observational analysis. *Nat. Commun.* **5**, 3098 (2014).
18. Wang, Y. et al. Assessing the effects of anthropogenic aerosols on Pacific storm track using a multiscale global climate model. *Proc. Natl. Acad. Sci. USA* **111**, 6894–6899 (2014).
19. Lu, Y. & Deng, Y. Impact of environmental aerosols on a developing extratropical cyclone in the Superparameterized community atmosphere model. *J. Clim.* **29**, 5533–5546 (2016).
20. Zhou, R. & Deng, Y. A model analysis of the interactions between East Asian anthropogenic aerosols and North Pacific atmospheric transients in boreal winter. *J. Geophys. Res. Atmos.* **118**, 306–316 (2013).
21. Schreiber, E. A. P. & Serreze, M. C. Impacts of synoptic-scale cyclones on Arctic sea-ice concentration: a systematic analysis. *Ann. Glaciol.* **61**, 139–153 (2020).
22. Svendsen, L., Keenlyside, N., Bethke, I., Gao, Y. & Omrani, N.-E. Pacific contribution to the early twentieth-century warming in the Arctic. *Nat. Clim. Change* **8**, 793–797 (2018).
23. Zhang, J., Lindsay, R., Schweiger, A. & Steele, M. The impact of an intense summer cyclone on 2012 Arctic sea ice retreat. *Geophys. Res. Lett.* **40**, 720–726 (2013).
24. Boreddy, S. K. R. & Haque, M. M. & Kawamura, K. Long-term (2001–2012) trends of carbonaceous aerosols from a remote island in the western North Pacific: an outflow region of Asian pollutants. *Atmos. Chem. Phys.* **18**, 1291–1306 (2018).
25. Moreno, T. et al. Natural versus anthropogenic inhalable aerosol chemistry of transboundary East Asian atmospheric outflows into western Japan. *Sci. Total Environ.* **424**, 182–192 (2012).
26. Gelaro, R. et al. The Modern-Era retrospective analysis for research and applications, version 2 (MERRA-2). *J. Clim.* **30**, 5419–5454 (2017).
27. Chang, E. K. M., Lee, S. & Swanson, K. L. Storm track dynamics. *J. Clim.* **15**, 2163–2183 (2002).
28. Chang, E. K. M., Guo, Y. & Xia, X. CMIP5 multimodel ensemble projection of storm track change under global warming. *J. Geophys. Res. Atmos.* **117**, D23118 (2012).
29. Graff, L. S. & LaCasce, J. H. Changes in the extratropical storm tracks in response to changes in SST in an AGCM. *J. Clim.* **25**, 1854–1870 (2012).
30. Yin, J. H. A consistent poleward shift of the storm tracks in simulations of 21st century climate. *Geophys. Res. Lett.* **32**, L18701 (2005).

31. Wang, H. et al. Atmosphere teleconnections from abatement of China aerosol emissions exacerbate Northeast Pacific warm blob events. *Proc. Natl. Acad. Sci. USA* **121**, e2313797121 (2024).
32. Liu, X. et al. Toward a minimal representation of aerosols in climate models: description and evaluation in the Community Atmosphere Model CAM5. *Geosci. Model Dev.* **5**, 709–739 (2012).
33. Tamarin, T. & Kaspi, Y. The poleward shift of storm tracks under global warming: a Lagrangian perspective. *Geophys. Res. Lett.* **44**, 666–10,674 (2017).
34. Coronel, B., Ricard, D., Rivière, G. & Arbogast, P. Role of moist processes in the tracks of idealized midlatitude surface cyclones. *J. Atmos. Sci.* **72**, 2979–2996 (2015).
35. Oruba, L. & Lapeyre, G. & Rivière, G. On the northward motion of midlatitude cyclones in a barotropic meandering jet. *J. Atmos. Sci.* **69**, 1793–1810 (2012).
36. Oruba, L., Lapeyre, G. & Rivière, G. On the poleward motion of midlatitude cyclones in a baroclinic meandering jet. *J. Atmos. Sci.* **70**, 2629–2649 (2013).
37. Tamarin, T. & Kaspi, Y. The poleward motion of extratropical cyclones from a potential vorticity tendency analysis. *J. Atmos. Sci.* **73**, 1687–1707 (2016).
38. Rosenfeld, D. Suppression of rain and snow by urban and industrial air pollution. *Science* **287**, 1793–1796 (2000).
39. Khain, A., Rosenfeld, D. & Pokrovsky, A. Aerosol impact on the dynamics and microphysics of deep convective clouds. *Q. J. R. Meteorol. Soc.* **131**, 2639–2663 (2005).
40. van den Heever, S. C., Stephens, G. L. & Wood, N. B. Aerosol indirect effects on tropical convection characteristics under conditions of radiative–convective equilibrium. *J. Atmos. Sci.* **68**, 699–718 (2011).
41. Fan, J., Wang, Y., Rosenfeld, D. & Liu, X. Review of aerosol-cloud interactions: mechanisms, significance, and challenges. *J. Atmos. Sci*. **73**, 4221–4252 (2016).
42. Heikenfeld, M., White, B., Labbouz, L. & Stier, P. Aerosol effects on deep convection: the propagation of aerosol perturbations through convective cloud microphysics. *Atmos. Chem. Phys.* **19**, 2601–2627 (2019).
43. Li, X., Zhang, Q. & Xue, H. The role of initial cloud condensation nuclei concentration in hail using the WRF NSSL 2-moment microphysics scheme. *Adv. Atmos. Sci.* **34**, 1106–1120 (2017).
44. Rosenfeld, D. et al. Flood or drought: how do aerosols affect precipitation? *Science* **321**, 1309–1313 (2008).
45. Tao, W.-K., Chen, J.-P., Li, Z., Wang, C. & Zhang, C. Impact of aerosols on convective clouds and precipitation. *Rev. Geophys.* **50**, RG2001 (2012).
46. Dee, D. P. et al. The ERA-Interim reanalysis: configuration and performance of the data assimilation system. *Q. J. R. Meteorol. Soc.* **137**, 553–597 (2011).
47. Remer, L. A. et al. The MODIS aerosol algorithm, products, and validation. *J. Atmos. Sci.* **62**, 947–973 (2005).
48. Allen, R. J. & Sherwood, S. C. The impact of natural versus anthropogenic aerosols on atmospheric circulation in the Community Atmosphere Model. *Clim. Dyn.* **36**, 1959–1978 (2011).
49. Chen, G., Wang, W.-C. & Chen, J.-P. Circulation responses to regional aerosol climate forcing in summer over East Asia. *Clim. Dyn.* **51**, 3973–3984 (2018).
50. Gettelman, A. et al. Global simulations of ice nucleation and ice supersaturation with an improved cloud scheme in the Community Atmosphere Model. *J. Geophys. Res.* **115**, D18216 (2010).
51. Gettelman, A., Morrison, H., Santos, S., Bogenschutz, P. & Caldwell, P. M. Advanced two-moment bulk microphysics for global models. Part II: global model solutions and aerosol–cloud interactions. *J. Clim.* **28**, 1288–1307 (2015).
52. Park, S., Bretherton, C. S. & Rasch, P. J. Integrating cloud processes in the Community Atmosphere Model, Version 5. *J. Clim.* **27**, 6821–6856 (2014).
53. Neale, R. B. et al. Description of the NCAR Community Atmosphere Model (CAM 5.0). *NCAR Tech*. Note Ncar/tn-486+ STR, **1**, 1–12 (2010).
54. Lamarque, J.-F. et al. Historical (1850–2000) gridded anthropogenic and biomass burning emissions of reactive gases and aerosols: methodology and application. *Atmos. Chem. Phys.* **10**, 7017–7039 (2010).
55. Field, P. R. et al. Midlatitude cyclone compositing to constrain climate model behavior using satellite observations. *J. Clim.* **21**, 5887–5903 (2008).
56. Yettella, V. & Kay, J. E. How will precipitation change in extratropical cyclones as the planet warms? Insights from a large initial condition climate model ensemble. *Clim. Dyn.* **49**, 1765–1781 (2017).
57. Serreze, M. C. Climatological aspects of cyclone development and decay in the Arctic. *Atmos. Ocean* **33**, 1–23 (1995).
58. Wang, X. L., Feng, Y., Chan, R. & Isaac, V. Inter-comparison of extra-tropical cyclone activity in nine reanalysis datasets. *Atmos. Res.* **181**, 133–153 (2016).
59. Gilet, J.-B. & Plu, M. & Rivière, G. Nonlinear baroclinic dynamics of surface cyclones crossing a zonal jet. *J. Atmos. Sci.* **66**, 3021–3041 (2009).
60. Rossby, C. G. On displacements and intensity changes of atmospheric vortices. *J. Mar. Res.* **7**, 175–187 (1948).
61. Emanuel, K., Fantini, M. & Thorpe, A. Baroclinic instability in an environment of small stability to slantwise moist convection. Part I: two-dimensional models. *J. Atmos. Sci.* **44**, 1559–1573 (1987).

Acknowledgements

This study and D.C. were supported by the Excellent Research Group Program for Tibetan Plateau Earth System (Grant No. 42588201). D.C. was also supported by the National Natural Science Foundation of China (Grant No. U2442213). Y.L. was supported by the National Natural Science Foundation of China (Grant No. 42130603). Y.D. was supported by the U.S. National Science Foundation (NSF) through Grant No. AGS-2032532 and by the U.S. National Oceanic and Atmospheric Administration (NOAA) through Grant No. NA22OAR4310606. We also thank the editor and the two anonymous reviewers for their thoughtful and constructive comments, which significantly improved the quality of this paper.

Author contributions

Y.L. suggested the study. Y.L., D.C., Y.D., Q.Z., and X.Z. designed the modeling and analysis strategy. D.C. conducted modeling experiments and led the model analysis, figure production and writing of the manuscript. D.C., D.X., X.C., and M.G. contributed to discussions and the improvement of the manuscript. All authors have approved the final manuscript.

Competing interests

The authors declare no competing interests.

Additional information

Supplementary information The online version contains supplementary material available at https://doi.org/10.1038/s41612-026-01377-w.

Correspondence and requests for materials should be addressed to Yanluan Lin or Yi Deng.